Acceleration of Chemical Reaction in Boiling Polymer Solutions

L. Chen, G. H. Hu, and J. T. Lindt
Dept. of Material Science and Engineering, University of Pittsburgh, Pittsburgh, PA 15261

This article discusses the effect of boiling inert hydrocarbon solvent on the model second-order transesterification reaction of ethylene/vinyl acetate copolymer with 3-phenyl 1-propanol. In the presence of boiling, the overall reaction rate increases substantially due to mass-transfer effects in the proximity of the vapor-liquid interface. The present experiments and theory indicate that during the lifetime of a bubble in the boiling medium, the concentrations of reactants and the catalyst increase significantly near the bubble surface due to the rapid diffusion of the inert solvent. After the bubble rupture, the concentration differences persist and continue affecting the chemical reaction rate. The combination of these effects is responsible for the apparent increase in the overall reactivity.

Introduction

Solvents are frequently introduced into reacting polymer systems to facilitate molecular diffusion and heat transfer in the reactor. Such operations are usually carried out below the boiling point(s) of the solvents present. It can be expected that, when boiling is introduced, additional mixing occurs due to bubble growth and collapse. The presence of a boiling solvent can further reduce the temperature differences throughout the reacting medium and, equally importantly, provide internal means of selective temperature control.

The formation and growth of bubbles affect both the bulk mixing and the local conditions at the vapor-liquid interface where significant mass fluxes exist. Of particular interest are the synergistic effects between the apparent reactivity of the system and mass transfer expected to arise under such conditions. Specifically, the reaction conditions near the bubble surface and the carryover effect after the bubble collapse at the surface of the reacting medium will be considered.

The main objectives of this article are: to establish experimental evidence that boiling indeed can affect appreciably the overall rate of a chemical reaction and to provide a semiquantitative interpretation of the synergism between devolatilization and nonlinear reaction kinetics in a reacting polymeric system containing boiling solvents.

The reaction rate of the transesterification of EVA with 3-phenyl 1-propanol was found to almost double in the boiling solvent while no changes in reaction mechanism were observed. This effect on the reaction acceleration was explained by locally enhanced mass transfer originating at the bubble interface, which was interpreted mathematically in terms of bubble growth in a multicomponent solution, subsequent rupture and contraction of the bubble interface film and the diffusion processes accompanying these events.

The dynamics of the bubble growth has been extensively studied. For example, Scriven (1959) developed models for the bubble growth in a pure boiling liquids and binary solutions, Han (1981) and Amon (1984) presented models for bubble growth in binary polymer solutions. In this work, a multicomponent reacting system is introduced to explain the reaction acceleration observed.

Model Reaction

To examine the mass-transfer effects on the apparent reactivity of a boiling polymer solution, a transesterification reaction between poly(ethylene-covinyl acetate) and an alcohol has been used. This reversible, second-order reaction can be represented by the following overall scheme:

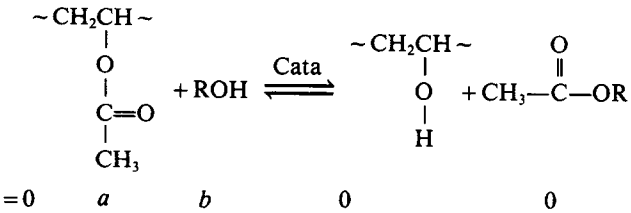

$t=0$	a	b	0	0
$t>0$	$a(1-p)$	$b-ap$	ap	ap

Correspondence concerning this article should be addressed to J. T. Lindt.

where a and b denote the initial concentrations of the vinyl acetate and the vinyl alcohol groups, and p is the overall conversion based on the acetate group concentration. The overall reaction rate is given by:

$$-\frac{d(a-ap)}{dt}=k_1(a-ap)(b-ap)-k_2(ap)(ap) \quad (1)$$

where k_1 and k_2 are the forward and reverse reaction rate constants, respectively. Upon introducing the functional ratio, $r^*=b/a$, Eq. 1 can be simplified to:

$$\frac{dp}{dt}=k_1a(1-p)(r^*-p)-k_2ap^2 \quad (2)$$

The equilibrium constant K_e can be determined either from the equilibrium conversion, p_e, or calculated from k_1 and k_2:

$$K_e=\frac{p_e^2}{(1-p_e)(r^*-p_e)}=\frac{k_1}{k_2} \quad (3)$$

In the analysis to follow, Eqs. 2 and 3 are used as the governing overall kinetic equations for the transesterification reaction.

In the context of this work, it is important to note that the reaction rate constants were found to be independent of both the amount of solvent and the rate of mechanical agitation, including conditions when no solvent was added (Hu, 1992). Thus, this reaction is slow enough to rule out mixing effects in the absence of bubbles.

All other pertinent details are given elsewhere (Hu, 1992).

Table 1. Selected Properties of Alcohol and Solvents

	Molec. Wt. (g/mol)	Melting Point (°C)	Boiling Point (°C)
PPOH	136.19	−18	235
DBTDL	631.56	—	—
1-octane	114.23	−57	126
1-nonane	128.26	−53	151
1-decane	142.29	−30	174
1-dodecane	170.34	−12	216

Experimental Studies

Materials

The ethylene and vinyl acetate copolymer (EVA) used in this study contains 14% of vinyl acetate units with a number mass molecular weight of 21,000 g/mol and a polydispersity of 3.5. 3-phenyl 1-propanol (PPOH) and dibutyl tin dilaurate (DBTDL) were chosen as the alcohol and the catalyst. As solvents, a series of homologous hydrocarbons was used, namely, 1-octane, 1-nonane, 1-decane, and 1-dodecane. Some selected properties of the alcohol and the solvents are shown in Table 1.

Procedures

The reaction was conducted in a stirred three-neck flask (0.5l) immersed in a thermostatted oil bath (Figure 1a). The temperature was controlled within ±0.2°C.

Boiling was introduced into the reacting medium by overheating the reactor (the temperature of the oil bath was kept at 15°C higher than the boiling point of the reacting solution),

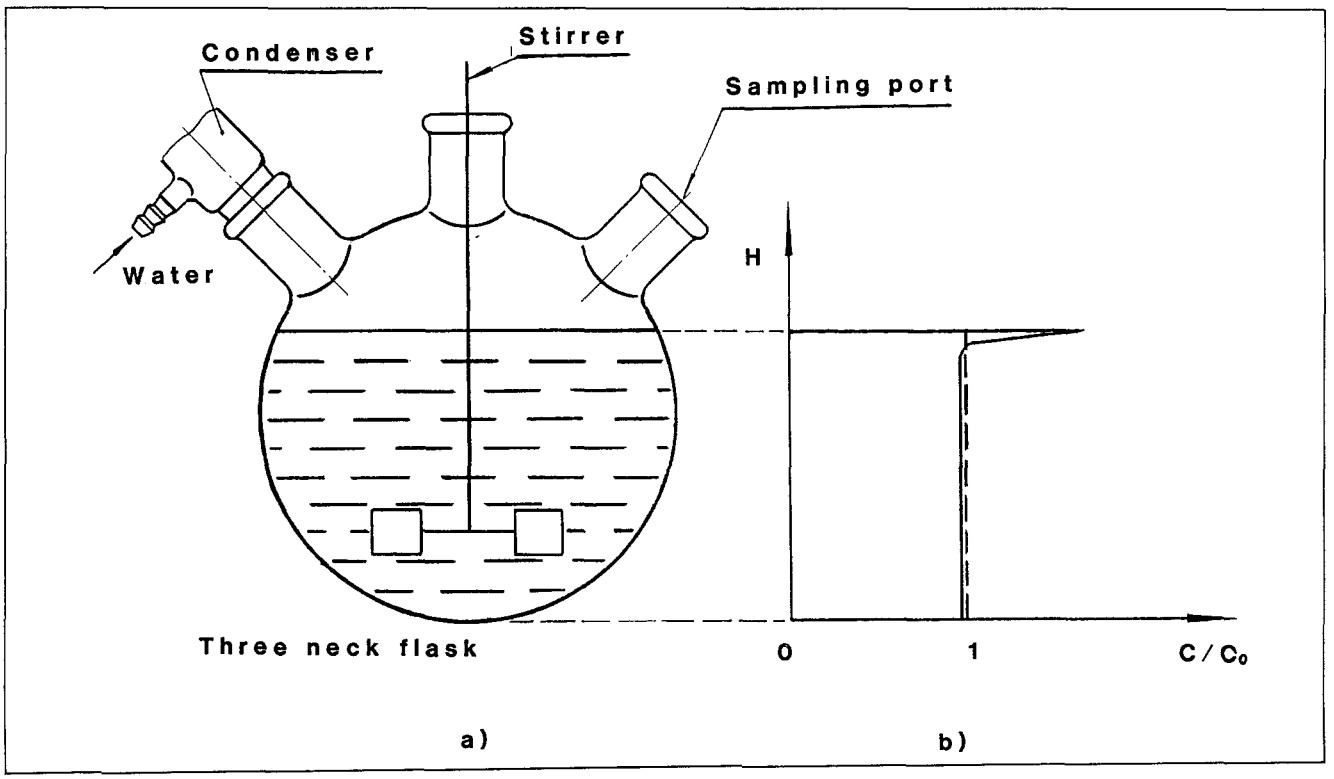

Figure 1. Polymer concentration profile in a boiling solution: a) reactor; b) concentration profile.

while a sufficient amount of boiling stones was added. The vapor was condensed in a condenser mounted on one of the necks of the flask and refluxed back into the reactor.

Conversion determination

To determine the overall conversion in the bulk of the reactor as a function of time, samples were drawn in regular intervals. The polymer was extracted from solution by precipitation in acetone, followed by filtration, redissolution in 1-octane, and reprecipitation in acetone. Before analysis, the polymer samples were dried at 80°C in a vacuum for at least 24 hours.

The conversion of the vinyl acetate group into the corresponding vinyl alcohol group was followed by a Fourier Transform Infrared spectrometer.

Concentration at the reactor surface

To examine the extent of solvent depletion at the bubbles' surface, separate experiments were conducted to collect samples from the reactor surface to which the bubbles rise and where they eventually rupture.

For this purpose, the three-neck reactor containing a 20% polystyrene (PS) solution in tetrahydrofuran (THF) was placed in the oil bath at 15°C higher than the boiling point of the solvent. Samples were collected at different positions from the reactor surface as well as in the reactor bulk after 10 minutes of boiling.

The concentrations of PS in the samples were determined by UV analysis, thus providing a crude estimation of the concentration profile across the depth of the reactor.

Theory

The mass transfer and chemical reaction in a boiling solution are associated with a broad spectrum of concentration gradients. Particular attention is paid to the situations that explicitly involve the steep gradients originating at the vapor-liquid interface. There, three distinct hydrodynamic environments for mass transfer are involved, as connected to the consecutive events of bubble growth, bubble rupture, and incorporation of the ruptured bubble interface film (defined as a liquid shell around the bubble containing higher concentrations of reactants) back into the solution.

Two distinct mass-transfer regimes are considered in the sequence, which arise during the *bubble lifetime* and after the *bubble collapse*. The hydrodynamics is treated only to the extent necessary for a solution of the mass-transfer problem.

Mass transfer prior to bubble rupture

The cell model for bubble growth given in this section is developed to explain the onset of the concentration gradients near the vapor-liquid interface.

The bubble growth in binary systems, including polymer solutions, has been studied previously. In distinction to the previous work, this work employs a polymeric system that contains an inert solvent, a soluble reacting alcohol, a soluble catalyst, and the ester split out by the reaction. The cell model presented here accounts for the presence of multiple species.

The liquid is conceptually divided into cells that have the same size as the radius of R_v, and each cell contains a single bubble with radius R (Figure 2). The bubble growth is assumed to be controlled by diffusion.

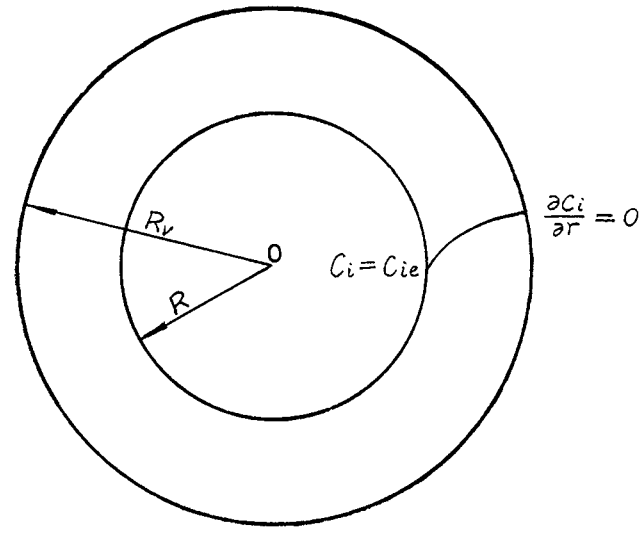

Figure 2. Cell model for the bubble growth.

Equation of diffusion

The equation of diffusion for a multicomponent system (containing $n+1$ components) takes the following form in spherical coordinates:

$$\frac{\partial C_i}{\partial t}+u_r\frac{\partial C_i}{\partial r}+\frac{u_\theta}{r}\frac{\partial C_i}{\partial \theta} + C_i\sum_{j\neq i}^{n}\frac{1}{\rho_j}\left(\frac{\partial C_j}{\partial t}+u_r\frac{\partial C_j}{\partial r}+\frac{u_\theta}{r}\frac{\partial C_j}{\partial \theta}\right)=\sum_{j=1}^{n}\nabla\cdot D_{ij}\nabla C_j \quad (4)$$

where C_i is the concentration of component i in kg/m^3, and D_{ij} is the diffusivity. For unidirectional diffusion, assuming that the main terms of diffusivity, D_{ii}, are much larger than the interactional terms D_{ij} (Cussler, 1976), Eq. 4 reduces to:

$$\frac{\partial C_i}{\partial t}+u_r\frac{\partial C_i}{\partial r}+\frac{u_\theta}{r}\frac{\partial C_i}{\partial \theta} + C_i\sum_{j\neq i}^{n}\frac{1}{\rho_j}\left(\frac{\partial C_j}{\partial t}+u_r\frac{\partial C_j}{\partial r}+\frac{u_\theta}{r}\frac{\partial C_j}{\partial \theta}\right)=\frac{D_{ii}}{r^2}\frac{\partial}{\partial r}\left(r^2\frac{\partial C_i}{\partial r}\right) \quad (5)$$

Upon introducing a moving coordinate r' along with the fact that the velocity in r direction $u_r=(dR/dt)(R^2/r^2)$ (see Eq. 14):

$$r'=r+u_r t=r+\dot{R}\frac{R^2}{r^2}t \quad (6)$$

and dropping the apostrophe for brevity, the final form of the diffusion equation is obtained:

$$\frac{DC_i}{Dt}+C_i\sum_{j\neq i}^{n}\frac{1}{\rho_j}\left(\frac{DC_j}{Dt}\right)=\frac{D_{ii}}{r^2}\frac{\partial}{\partial r}\left(r^2\frac{\partial C_i}{\partial r}\right) \quad (7)$$

where r is now a *moving coordinate*. (The convection terms

due to the vertical translation of the bubble motion are negligible. An approximate calculation using the Stokes' law and Eq. 7 indicates that, within about 20 μm of the bubble surface, these terms are much smaller than the radial convective term.)

Note that the second term on the lefthand side of Eq. 7 (and the corresponding terms in Eqs. 4 and 5) does not arise for binary systems. This term accounts for the change in concentration of component i due to diffusion of the *other components* j ($j=1, 2, 3, ..n$). Derivation of this term is detailed in the Appendix.

Equation 7 is subject to the initial condition (Eq. 8) and the boundary conditions (Eqs. 9–10):

$$C_i(r, 0) = C_{i0} \tag{8}$$

$$C_i(R, t) = C_{ie} \tag{9}$$

$$\left(\frac{\partial C_i}{\partial r}\right)_{r=R_v} = 0 \tag{10}$$

where C_{i0} is the initial concentration of the component i, C_{ie} is the equilibrium concentration of the component i inside the bubble, R is the instantaneous radius of the bubble, and R_v is the radius of the cell. The equilibrium concentration of the component i (C_{ie}) is determined by Flory-Huggins relations, written currently for a three-component system (Flory, 1953): the polymer, the nonvolatile reactant, and the volatile solvent.

When a chemical reaction is introduced, Eq. 7 becomes:

$$\frac{DC_i}{Dt} + C_i \sum_{j\neq i}^{n} \frac{1}{\rho_j}\left(\frac{DC_j}{Dt}\right) = \frac{D_{ii}}{r^2}\frac{\partial}{\partial r}\left(r^2\frac{\partial C_i}{\partial r}\right) - \frac{\partial S_i}{\partial t} \tag{11}$$

The second term in the right side of Eq. 11 accounts for the rate of the concentration change of the reactive component i due to reaction. It follows from the stoichiometry:

$$\frac{\partial S_i}{\partial t} = M a \nu_i \frac{dp}{dt} \tag{12}$$

where M is the molecule weight of component i, a is the initial molar concentration of vinyl acetate, and ν_i is the stoichiometric ratio. The conversion rate, dp/dt, is given by Eq. 2.

Equation of motion

A unidirectional flow field around the bubble is assumed:

$$\vec{u} = [u_r(r), 0, 0] \tag{13}$$

We further assume the solution to be incompressible:

$$u_r = \dot{R}\frac{R^2}{r^2} \tag{14}$$

and thus, for a Newtonian liquid, the stress tensor can be written by:

$$\tilde{\tau} = \dot{R}\frac{R^2}{r^3}\begin{pmatrix} -4\mu & 0 & 0 \\ 0 & 2\mu & 0 \\ 0 & 0 & 2\mu \end{pmatrix} \tag{15}$$

Combining the equation of motion and the requirement of mechanical equilibrium on the bubble surface, the well-known relation for bubble growth is obtained:

$$p_R - p_\infty = \rho\left(\frac{3}{2}\dot{R}^2 + R\ddot{R}\right) + \frac{2\sigma}{R} + \frac{4\mu\dot{R}}{R} \tag{16}$$

to be solved with the initial conditions:

$$R(0) = R_0; \quad \dot{R}(0) = 0 \tag{17}$$

The viscosity of the solution is assumed to be Newtonian and to be a function of concentration and temperature only (Mutschler, 1991):

$$\mu = \mu_0 C^\beta \exp[(\Delta E - mC)/R_g T] \tag{18}$$

where C is the average concentration of the polymer in the cell, β and m are empirical constants, and T is the temperature.

The calculations indicate that the inertia term in Eq. 16 is negligibly small, and hence the equation for bubble growth becomes:

$$p_R - p_\infty = \frac{2\sigma}{R} + \frac{4\mu\dot{R}}{R} \tag{19}$$

Mass balance on the bubble

The differential mass balance on the bubble relates the bubble radius to the diffusive flux:

$$\frac{d}{dt}\left(\frac{4}{3}\pi R^3 \rho_g\right) = 4\pi R^2 \sum_{i=1}^{n-1}\left[D_{ii}\left(\frac{\partial C_i}{\partial r}\right)_{r=R}\right] \tag{20}$$

where C_i is the concentration of the component i in kg/m^3, and ρ_g is the density of the gas inside the bubble, namely,

$$\rho_g = \frac{p_R \sum_{i=1}^{n-1}(x_i M_i)}{R_g T} \tag{21}$$

where p_R is the pressure inside the bubble, x_i is the molar fraction of component i in the gas inside the bubble, and M_i is the molecular weight of component i.

In the solution algorithm, an integral form of the mass balance is used. The integral form of the mass balance for a multicomponent system gives:

$$\frac{4}{3}\pi(R^3\rho_g - R_0^3\rho_{g0}) = \sum_{i=1}^{n-1}\left(V_0 C_{i0} - \int_R^{R_v} 4\pi r^2 C_i dr\right) \tag{22}$$

remembering that r is the moving coordinate and C_i is expressed as a function of the moving coordinate.

Mass transfer after bubble rupture

During rapid vaporization of solvents in polymer solutions, vapor bubbles grow and approach the free surface and rupture. As a result of the rapid diffusion of the volatile solvent in the nonvolatile mixture of the reactants and of the catalyst, a highly

concentrated and reactive layer at the bubble liquid interface tends to develop. After rupture, the relatively viscous meniscus that contains the residual of the bubble interface film is deposited on the surface of the reacting solution, subject to continued reaction and to diffusive mass exchange. In this section, the hydrodynamic events during and after the bubble rupture are examined but limited to the extent relevant to mass transfer.

It is suggested that after the bubble rupture at the solution free surface, the convex bubble interface film contracts quickly, driven by surface forces. During the contraction, the thickness increases greatly, thus tending to preserve the high concentration for a relatively long time and making it available for further enhancement of the chemical reaction. The contribution of these events to the overall chemical conversion is examined below.

Figure 3 charts schematically the bubble rupture process (*a-e*) as well as a proposed physical model for the bubble contraction after rupture (*f-h*). Two separate problems are treated below:

- Contraction of the meniscus into a droplet in the absence of reaction
- Mass transfer and reaction in a motionless droplet.

Hydrodynamics of bubble rupture

To obtain a crude estimate of the time needed for the convex meniscus to contract into a spheroidal droplet, the meniscus shape has been approximated by a flat disc of a diameter equal to the bubble diameter prior to rupture and of a thickness equal to the critical thickness (Figure 4). It is further assumed that the liquid is incompressible and of constant viscosity, and that the minor velocity component, u_z, is independent of the radial position, r.

The equation of continuity:

$$\frac{1}{r}\frac{\partial}{\partial r}(\rho r u_r)+\frac{\partial}{\partial z}(\rho u_z)=0 \tag{23}$$

along with the boundary condition:

$$r=R:\quad u_r=\dot{R} \tag{24}$$

leads to an estimate of the radial velocity:

$$u_r=\dot{R}\frac{r}{R} \tag{25}$$

When Eq. 25 is substituted into the equation of motion:

$$\rho\left(\frac{\partial u_r}{\partial t}+u_r\frac{\partial u_r}{\partial r}\right)=-\frac{\partial p}{\partial r}+\mu\frac{\partial}{\partial r}\left(\frac{1}{r}\frac{\partial}{\partial r}(ru_r)\right) \tag{26}$$

and subject to integration from $r=0$ to $r=R$, an explicit equation for the radius of the disc, R, is obtained:

$$\frac{\rho}{2}(\ddot{R}R+\dot{R}^2)=p_0-p_{R-0} \tag{27}$$

Mechanical equilibrium over the disc edge requires that:

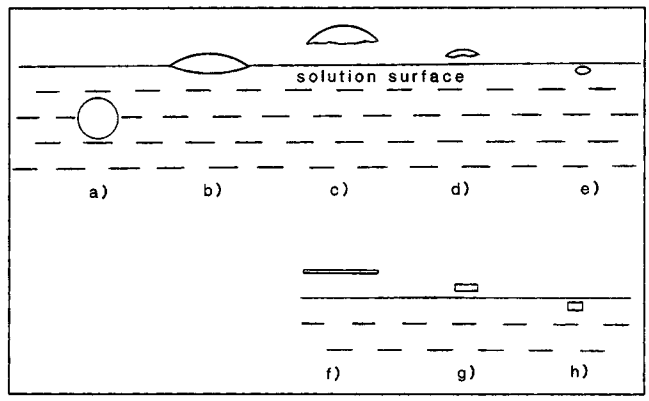

Figure 3. Bubble rupture process (a-e) and overall physical model (f-h).

$$p_{R-0}-p_{R+0}-\frac{\sigma}{\delta}-2\mu\frac{\dot{R}}{R}=0 \tag{28}$$

Finally, when Eqs. 27 and 28 are combined, the rate of contraction of the liquid meniscus can be determined from:

$$\frac{\rho}{2}(\ddot{R}R+\dot{R}^2)=-\frac{\sigma}{\delta}-2\mu\frac{\dot{R}}{R} \tag{29}$$

with the initial conditions:

$$R(0)=R_f;\quad \dot{R}(0)=0;\quad \delta(0)=\delta_0 \tag{30}$$

where R_f is the bubble radius before rupture and δ_0 is the critical bubble wall thickness at rupture.

The critical thickness before bubble rupture was estimated by mass balance from the experimental results for the polymer concentration profile in the top layer in the reactor (Figure 1b) and the predicted results for the polymer concentration profile in the bubble cell (Figure 5b).

The highest concentration in the sample drawn from the top layer, say 0.5 mm thick, is 61% higher than the bulk concentration. In other words, the average concentration in the rup-

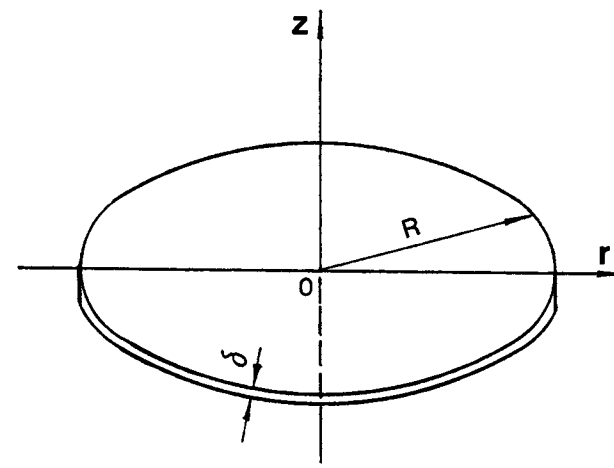

Figure 4. Physical model for the contraction of bubble interface film.

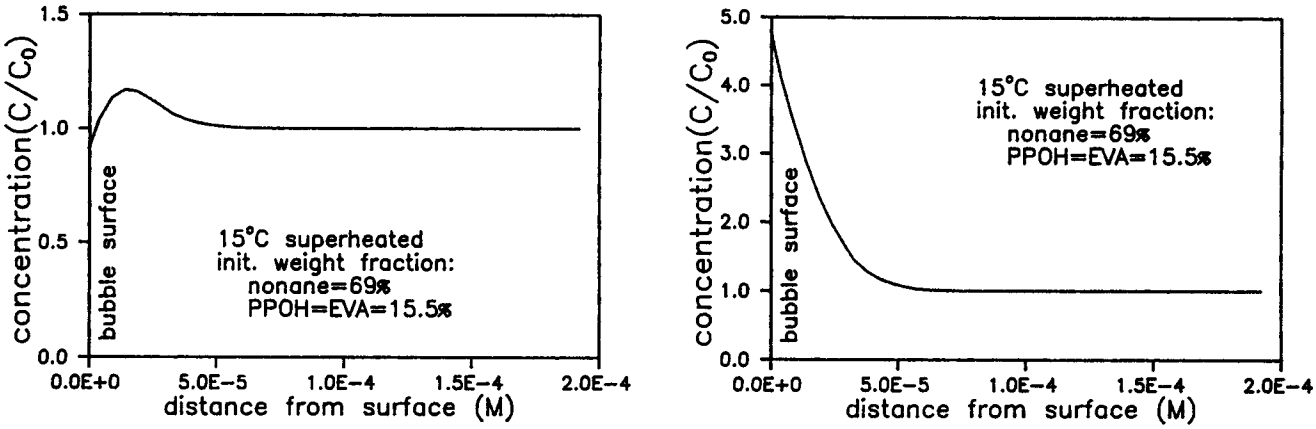

Figure 5. Concentration profile in the bubble cell: a) PPOH; b) polymer and catalyst.

tured bubble skin must be higher than or equal to this figure. It is clear that this average concentration is a function of the critical thickness of the bubble wall at rupture (see Figure 5b, the polymer concentration profile in the bubble cell). The mass-balance calculation based on Figure 5b indicated that the critical thickness must be less than 20 μm.

The lower limit of the critical thickness can be estimated by the cumulative polymer concentration increase in the top layer. The thickness of the top layer probed was about 3 mm with the average concentration 41% higher than the bulk concentration after 10 minutes of boiling (see the section on Experimental Studies). The mass-balance calculations based on Figure 5b and the estimated nucleation rate from visual observations, about 600 nuclei/L/s, suggest that the critical thickness must be larger than 3.3 μm.

In the calculation concerning the bubble rupture, Eqs. 29, 30, 31, 32 and 33, the critical thickness is assumed to be 10 μm.

Diffusion in the contracted meniscus

For a disk-shaped droplet, considered in the preceding paragraph and shown in Figure 3, the one-dimensional equation of diffusion can be used to estimate the concentration profile across the thickness, z, assuming thus after contraction negligible concentration differences along the radius of the disc, r:

$$\frac{\partial C_i}{\partial t} + C_i \sum_{j \neq i}^{n} \frac{1}{\rho_j}\left(\frac{\partial C_j}{\partial t}\right) = D_{ii}\frac{\partial^2 C_i}{\partial z^2} \tag{31}$$

The convective diffusion terms were omitted, thus implying that mechanical mixing does not affect molecular diffusion, as substantiated below.

The initial concentration profile is assumed to be determined by the concentration profile established in the bubble wall prior to rupture, and thus simply obtained by rescaling it across the disc depth:

$$C_i(z, 0) = C_i^{B.R.}\left(z\frac{\delta_0}{\delta}\right) \tag{32}$$

where $C_i^{B.R.}$ is the concentration profile in the disc-shaped meniscus before the contraction, and δ_0 and δ are the thicknesses of the disk before and after the contraction. The Reynolds number for the contraction flow is sufficiently small to make this assumption reasonable ($Re<1$). [Equation 29 suggests that the ratio of the inertia and viscous forces is $(\rho/4\mu)(\dot{R}/R)(R\ddot{R}+\dot{R}^2)$.]

The boundary conditions are:

$$C_i(0, t) = C_{i0};\quad C_i(\delta, t) = C_{i0} \tag{33}$$

where C_{i0} is the average concentration of component i in the whole system.

Results and Discussion

Apparent reaction rate in boiling solution

Figure 6 shows the chemical conversion as a function of time in the boiling solutions of 1-octane, 1-nonane and 1-decane, respectively. Also plotted are the conversion curves calculated from the kinetic data obtained in 1-dodecane (boil-

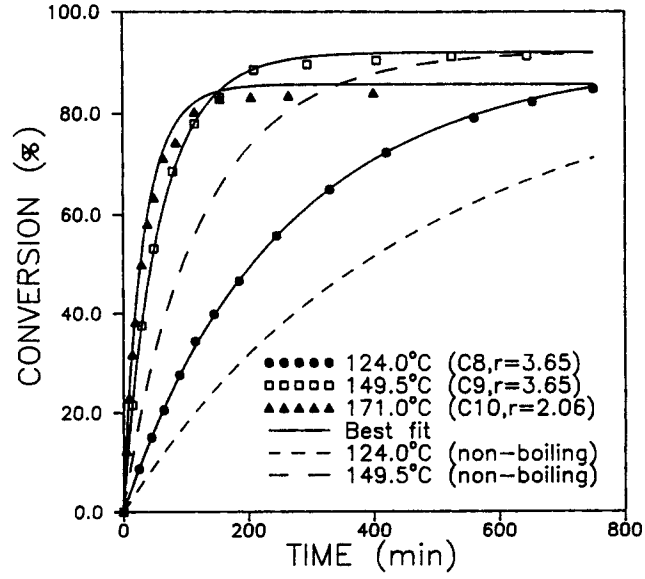

Figure 6. Conversion as a function of time in boiling solutions.

ing point = 216°C/760 mm Hg) solutions without boiling (Hu, 1992) for comparison. As can be seen, the reaction proceeds substantially faster in the boiling solutions, while the equilibrium states remain unchanged.

Additional results have shown that the reaction is not affected by the specific solvent within this homolog series of hydrocarbon solvents. It has also been seen that mechanical mixing has no effect on this particular reaction (Hu, 1992) as the reaction is sufficiently slow. [Hu reported that the kinetic behavior of this particular reaction is exactly the same in the bulk and in the nonboiling solution of 1-dodecane (Eq. 1).] Boiling does not change the reaction pathway. Equations 2 and 3 have been used to fit the experimental data obtained in boiling hydrocarbon solutions to obtain separate values of k_1 and k_2. A good fit of Eq. 2 to the experimental conversion values implies that the reaction in a boiling solution remains reversible and of second order (Figure 6). Also in agreement with the data obtained without boiling, the overall rate constants k_1 and k_2 obtained in boiling solutions are proportional to the square root of concentration of the catalyst (DBTDL), as indicated in Figure 7. We can therefore conclude that the reaction in nonboiling and boiling solutions follows the same pathway. An explanation of the greatly increased reaction rate in the presence of a boiling solvent ought to be sought in the physical phenomena connected to the presence of bubbles. (In fact, the apparent reaction rate depends on the degree of boiling, as suggested by data of Figure 8.)

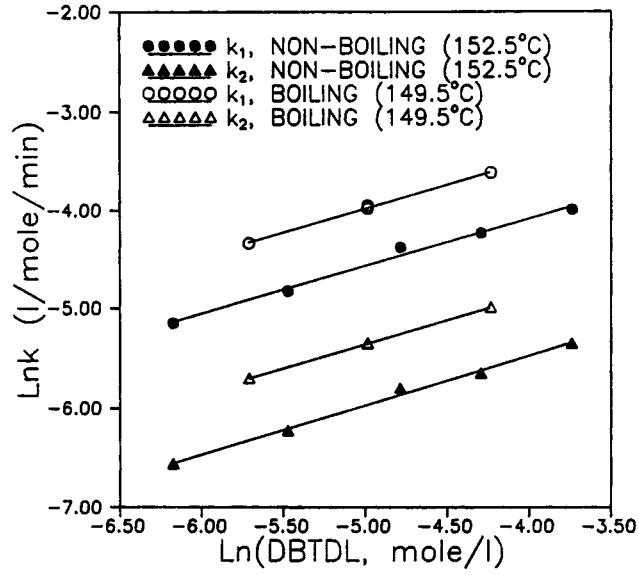

Figure 7. Effect of catalyst concentration on k_1 and k_2.

Effect of the vapor-liquid interface

The fact that the degree of boiling affects the overall reactivity of the solution (Figure 8) suggests that the enhancement of the apparent reaction rate is related to the magnitude of the vapor-liquid interface, and therefore to the number and size of the bubbles. As suggested above, both the bubbles physically present and their remnants in the form of the collapsed bubble interface films are related to the history of the vapor-liquid interface.

At the liquid side of the vapor-liquid interface, significant gradients of concentration and temperature are bound to arise. The concentration gradients are expected to be more significant, since the mass diffusivity, D_{ii}, is orders of magnitude smaller than the thermal diffusivity, α_H. The heat and mass balances over the bubble surface dictate that the concentration effects dominate as long as, say,

$$\frac{R_g T}{\Delta E}\frac{\alpha_H}{D_{ii}}\frac{n\rho C_p T}{\lambda C} \gg 1 \qquad (34)$$

where T is the mean temperature, ΔE the activation energy of reaction, n the apparent reaction order, ρ the solution density, C_p the solution specific heat, λ the vaporization heat, and C the concentration of the reactive groups. The validity of the results presented here are restricted by this condition.

The present cell model for bubble growth in a multicomponent system (Eqs. 4-22) predicts the concentration profiles in the expanding cell; Figure 5a shows an example for the concentration of the reacting alcohol (PPOH). It is interesting to find that, near the bubble surface, the concentration of reactant is much higher than the average concentration, in spite of the fact that PPOH is also removed into the bubble concurrently with the hydrocarbon solvent. As can be seen, the solvent which has a much lower boiling point is removed much more effectively than the reactant. Somewhat similar concentration profiles also exist for the polymer and the catalyst. Their molecules, however, are relatively large, and their diffusion rates are small. For this reason, the concentrations of the VA groups and the catalyst near the bubble surface are increased even more significantly than those of PPOH, as shown in Figure 5b.

Because the reaction rate depends on the concentration of the alcohol, polymer and catalyst, we can expect that the devolatilization process can locally accelerate the reaction. The intensity of this local concentration effect depends on a number of factors, but most notably on the relative rate of solvent

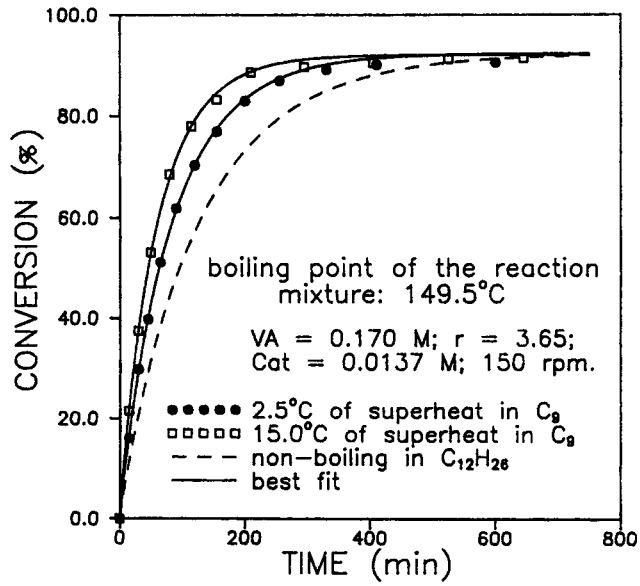

Figure 8. Effect of degree of boiling on the overall conversion.

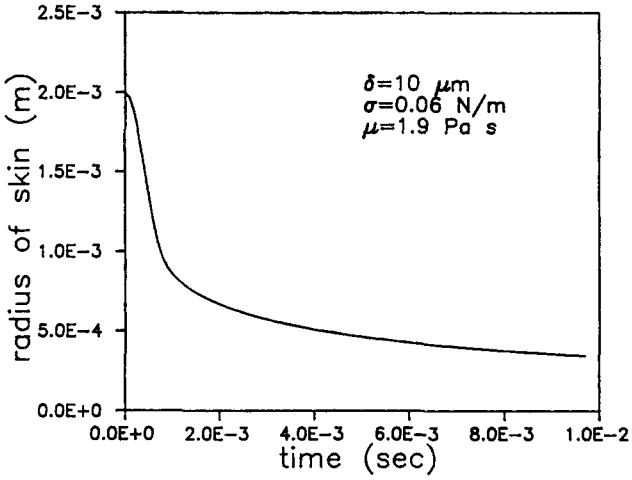

Figure 9. Contraction of the bubble interface film.

vaporization and on the order of reaction that remains a fixed parameter in this work.

Concentration distribution after bubble rupture

The bubble interface film, defined as a shell of liquid within which most of the concentration increase is contained, remains thin while the bubble is growing. Our calculations (Eqs. 4-22) suggest that the bubble interface film is typically less than 0.1 mm in thickness. As large as the concentration increase in the bubble interface film is, the relatively small liquid volume surrounding the growing bubbles alone is incapable of significant enhancement of the overall chemical reaction rate. It is the cumulative effect including the entire bubble population generated along the entire reaction path that is responsible for this effect.

The theory of mass transfer after the bubble rupture (Eqs. 31-33) indicates that the most important contribution to the enhancement of the overall reaction rate comes from the collapsed bubble interface films that remain segregated for a relatively long period of time.

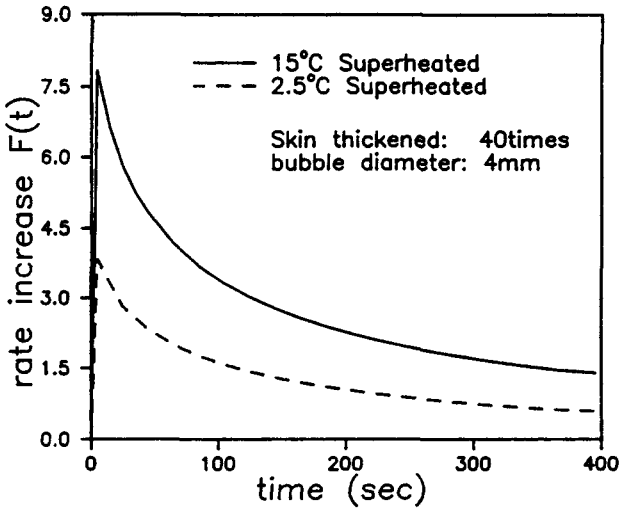

Figure 10. Reaction rate increase function *F(t)* for the growing bubble and contracted bubble interface film.

Once ruptured and subjected to surface forces, the bubble interface film contracts rapidly. Figure 9 shows the simulated bubble meniscus contraction process, utilizing a solution of Eqs. 29 and 30. The computations suggest that the radius of the bubble interface film contracts more than 6 times in less than 0.01 s: the time it may take the disengaged bubble interface film to fall back onto the solution surface. At the same time, the thickness of the bubble interface film, and thus the diffusion length, increases more than 40 times. It takes a long time for the concentration gradients within thus formed droplets to dissipate by molecular diffusion. It is unlikely that this process will be accompanied by significant mechanical mixing effects, mainly because the globules thus formed have a much higher viscosity than the rest of the solution. [Our measurements have shown that the viscosity of the EVA solution in nonane is proportional to the 5th power of the polymer concentration (Mutschler, 1991).] The freshly formed globules are placed in contact with older globules of similar initial composition to form a surface layer with a relatively high polymer concentration rather than being mixed into the bulk of the liquid.

This fact has been proven experimentally using the sampling technique described above. The UV analysis shows that, near the solution surface, the concentration is 61% higher than the concentration in the bulk and 43% higher when measured within a layer extending 2-3 mm below the surface. The bulk concentration is about 1-1.5% lower than the initial concentration because of the reflux of the solvent. Figure 1b shows the concentration profile in the solution inferred from these somewhat crude measurements.

In the absence of mixing, the concentration changes within the collapsed bubble interface film are solely due to molecular diffusion and hence can be predicted by Eqs. 31-33. To characterize the enhancement of chemical reaction in a *single globule* due to the increase of concentration, a rate increase function $F(t)$ is introduced:

$$F(t^*) = \frac{(k_i)_{b\ t=t^*} - (k_i)_{\text{homo}}}{(k_i)_{\text{homo}}} \tag{35}$$

where t^* is the time elapsed since nucleation of a given bubble, $(k_i)_b$ are the average apparent forward ($i=1$) and reverse ($i=2$) reaction rate constants for the solution in the bubble interface film, and $(k_i)_{\text{homo}}$ are the reaction rate constants at a reference state in a homogeneous solution of equal temperature and free of bubbles. The function $F(t)$ was obtained from Eq. 2 and Eqs. 31-33. Figure 10 shows $F(t)$ as a function of time from the bubble nucleation. The first part of the curve concerns the bubble growth, in which $F(t)$ increases quickly to a maximum (bubble rupture point). The second part of the curve concerns the bubble effect after rupture, in which $F(t)$ decreases slowly in magnitude. The integral of the function $F(t)$ is the contribution of a single bubble to the acceleration of reaction. Note that the most important contribution to the acceleration of the reaction comes after the bubble rupture.

Overall acceleration of the reaction

The boiling solution contains a large population of growing

bubbles and, more importantly, contains many more collapsed bubbles which form a surface layer with a higher concentration of reactants and catalyst. The collective effect of all these growing and collapsed bubbles on the chemical reaction is described by an overall reaction rate increase function $R(t)$ defined by:

$$R(t) = \frac{(k_i)_b^* - (k_i)_{\text{homo}}}{(k_i)_{\text{homo}}} \tag{36}$$

where t is the time elapsed since the reaction started. Definition of $R(t)$ is analogous to $F(t)$, except that $(k_i)_b$ is now the apparent reaction rate constants for the whole system including both the active bubbles and the bubbles collapsed previously. Every bubble contributes to $R(t)$ from the embryonic stage until long after its collapse when the remnants of the ruptured bubble interface film are fully reacted. Hence, the $R(t)$ can be obtained by superimposing the reaction effects of all growing and collapsed bubbles that have developed in the system:

$$R(t) = \int_0^t J(t')VF(t-t')dt' \tag{37}$$

here, $J(t)$ is the nucleation rate (number of bubbles nucleated per unit of volume per second) as a function of time since the reaction started, V is the volume of a single contracted bubble interface film, given by the critical thickness and the bubble size. $F(t)$ is the function defined by Eq. 35. In the calculations, $J(t')$ is assumed to be independent of time. Therefore, the bubbles population is constant, and all bubbles reach the same size before rupture, consequently V is a constant. Figure 11 shows the effect of bubbles generated at two different degrees of superheat on the overall reaction acceleration rate $R(t)$, both experimentally obtained and predicted by the cell model described above. Note that the higher the degree of superheat, the more significant the increase in the overall reaction rate $R(t)$. The qualitative agreement between the model and the experimental results suggests that the locally enhanced mass transfer during the bubble growth and after the rupture are the primary reasons for the increase in the overall reaction rate.

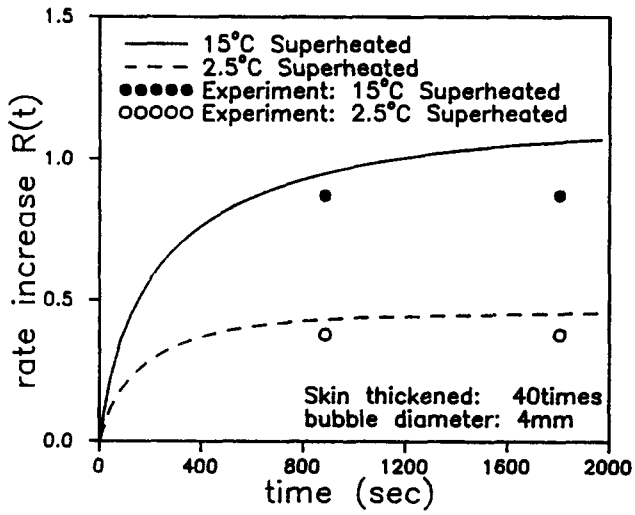

Figure 11. Overall reaction rate increase function *R(t)* for different values of the driving force.

In comparison to the experimental values of $R(t)$ obtained after 15 and 30 minutes of reaction, at which time the first two samples were taken, the predicted values are somewhat larger. The overestimation of the rate increase by the model can be possibly explained by the fact that this model omits completely the effect of convective diffusion. Mixing can be expected to accelerate the dissolution of the contracted bubble interface films back into the solution and interfere with these effects.

Concluding Remarks

The new experimental findings are as follows:

1. Boiling hydrcarbon solvents can appreciably enhance the overall reaction rate of the catalyzed transesterification of EVA. The acceleration in the reaction rate is not caused by changes in the reaction mechanism nor due to changes in the catalytic activity (Hu, 1992).

Although currently observed in one type of reactor, namely, a reflux stirred batch reactor, it can be expected that this effect is not limited to this particular experimental configuration, but that it exists in the general situation when boiling occurs in viscous systems where mixing is relatively poor.

The acceleration of the chemical reaction rate due to boiling has been made plausible by semiquantitative arguments based on the newly developed mathematical analysis for mass transfer during bubble growth, rupture, and after rupture.

2. The locally enhanced mass transfer in the liquid phase near the bubble surface, in a layer of the order of 10 μm thick, is the dominant reason for the reaction rate increase. The high mass-transfer rates are responsible for large concentrations of the reactants near the vapor-liquid interface. The intensity of this effect depends mainly on the reaction order and rate of vaporization of the solvent.

3. Under the present experimental conditions, the most important contribution to the reaction rate increase occurred after the bubble rupture. The relatively high concentrations of the reactants have been maintained in the bubble interface film after the bubble collapse. The time required for redissolution of the highly reactive bubble remnants into the solution is long enough for the remnants to affect the reaction rate significantly.

This work has firmly established that boiling can have a pronounced effect on the course of chemical reaction. In addition to providing additional means of controlling the overall heat transfer and mixing, it has been shown that boiling of an inert solvent can accelerate the apparent reaction rate due to mass-transfer phenomena arising in the vicinity of the continuously generated vapor-liquid interface.

Notation

a = initial molar concentration of vinyl acetate group, M
b = initial molar concentration of alcohol, M
C = bulk concentration of polymer, kg/m^3
C_i = concentration of component i, kg/m^3
C_{i0} = initial concentration of component i, kg/m^3
C_{ie} = equilibrium concentration of component i, kg/m^3
C_p = specific heat, J/kg·C°
D_{ii} = diffusion coefficient of component i, m^2/s
D_{ij} = interactional diffusion coefficient of component i and j, m^2/s

$F(t)$ = function defined by Eq. 35
$J(t)$ = nucleation function, $1/m^3 \cdot s$
k_{ci} = catalytic rate constant, $M^{-1.5} \cdot min^{-1}$
k_i = reaction rate constant, $M^{-1} \cdot min^{-1}$
K_e = equilibrium constant
M = molecular weight of PPOH, kg/mol
M_i = molecular weight of component i, kg/mol
n = reaction order
p = conversion, %
p_e = conversion at equilibrium, %
p_i = partial pressure of component i inside the bubble, Pa
p_i^0 = saturated vapor pressure for pure component i, Pa
p_R = pressure inside the bubble, Pa
p_∞ = operation pressure, Pa
r = coordinate or moving coordinate, m
r^* = functional ratio b/a
R = bubble or collapsed bubble interface film radius, m
R_0 = initial bubble radius, m
R_g = gas constant, 8.314 J/mol/K
R_v = radius of the bubble cell, m
$R(t)$ = function defined by Eq. 37
t = time, s
t^* = time elapsed since nucleation, s
T = temperature, K
u_r = velocity in r direction, m/s
V = volume of a contracted bubble interface film, m^3
V_0 = initial volume of the bubble cell, m^3
x_i = molar fraction of component i the gas inside the bubble

Greek letters

α_H = thermal diffusivity, m^2/s
β = power index for the concentration dependence of viscosity
ΔE = activation energy, J/mol
δ = thickness of the bubble interface film, m
λ = vaporization heat, J/kg
μ = viscosity, Pa·s
μ_0 = viscosity at reference concentration and temperature, Pa·s
ν_i = stoichiometric ratio of component i
ρ_i = density of component i, kg/m^3
ρ_g = gas density inside the bubble, kg/m^3
σ = surface tension, N/m
τ = stress, Pa

Literature Cited

Amon, M., and C. D. Denson, "Study of the Dynamics of Foam Growth: Analysis of the Growth of Closely Spaced Spherical Bubbles," *Polym. Eng. Sci.*, **24**, 1027 (1984).

Cussler, E. L., *Multicomponent Diffusion*, Elsevier Science Publishing, Oxford-New York (1976).

Flory, P. J., *Principles of Polymer Chemistry*, p. 548, Ithaca, NY (1953).

Han, C. D., and H. J. Yoo, "Studies on Structural Foam Processing: IV. Bubble Growth During Mold Filling," *Polym. Eng. Sci.*, **21**, 9 (1981).

Hu, G. H., J. T. Lindt, and M. Lambla, "Transesterification of Ethylene and Vinyl Acetate Copolymers with Alcohols in Solution and in the Bulk," *J. Appl. Polym. Sci.*, in press (1992).

Mutschler, R. A., "Effects of Concentration, Temperature, and Composition on the Viscosity of a Polymer Solution," BS Thesis, Dept. of MSE, Univ. of Pittsburgh (1991).

Scriven, L. E., "On the Dynamics of Phase Growth," *Chem. Eng. Sci.*, **10**, 1 (1959).

Appendix: Derivation of the Second Term in LHS of Eq. 4

In a system with $n+1$ components, the weight concentration of component i can be expressed:

$$C_i = \frac{G_i}{\sum_{j=1}^{n+1} G_j/\rho_j} \tag{A1}$$

When the composition of the system changes due to diffusion or reaction, the concentration change of component i can be obtained from:

$$\frac{DC_i}{Dt} = \lim_{\Delta t \to 0} \frac{1}{\Delta t}\left(\frac{G_i + \Delta G_i}{\sum_{j=1}^{n+1}(G_j + \Delta G_j)/\rho_j} - \frac{G_i}{\sum_{j=1}^{n+1} G_j/\rho_j}\right) \tag{A2}$$

Neglecting the higher-order differential terms, Eq. A2 becomes:

$$\frac{DC_i}{Dt} = \lim_{\Delta t \to 0} \frac{\Delta G_i - G_i \sum_{j=1}^{n+1} \Delta C_j/\rho_j}{\Delta t \sum_{j=1}^{n+1}(G_j + \Delta G_j)/\rho_j}$$

$$= \left[\frac{DC_i}{Dt}\right]^* - C_i \sum_{j \neq i}^{n} \frac{1}{\rho_j}\frac{DC_j}{Dt} \tag{A3}$$

The first and second terms in Eq. A3 are the contributions of the mass change in component i and in other components, respectively.

When the following diffusion equation:

$$\left[\frac{DC_i}{Dt}\right]^* = \nabla \cdot (D_{ii} \nabla C_i) \tag{A4}$$

is inserted into Eq. A3, Eq. 4 is obtained.

Manuscript received Feb. 20, 1992, and revision received Sept. 18, 1992.